International Journal of Heat and Mass Transfer 55 (2012) 8129–8138

Contents lists available at SciVerse ScienceDirect

International Journal of Heat and Mass Transfer

journal homepage: www.elsevier.com/locate/ijhmt

Pore shape development from a bubble captured by a solidification front

P.S. Wei *, S.Y. Hsiao [1]

Department of Mechanical and Electro-Mechanical Engineering, National Sun Yat-Sen University, 70 Lien-Hai Rd., District Ku-San, Kaohsiung 80424, Taiwan, ROC

ARTICLE INFO

Article history:
Received 11 June 2012
Received in revised form 27 August 2012
Accepted 27 August 2012
Available online 23 September 2012

Keywords:
Porosity
Pore formation
Solidification defect
Phase change
Pore shape
Bubble capture
Bubble entrapment

ABSTRACT

Development of the pore shape from a tiny bubble captured by a solidification front is fundamentally and systematically investigated in this study. Pore formation and its shape in solid influence not only microstructure of materials, but also contemporary issues of various sciences of biology, engineering, foods, geophysics and climate change, etc. In this work, the tiny bubble cap beyond the solidification front is considered to be spherical. As the dominant parameter, the bubble growth rate-solidification rate ratio, decreases, contact angle is found to approach 90°. An accepted criterion, stating that a pore becomes closed as long as the solidification rate is greater than bubble growth rate, is incorrect. This study also finds that the pore can be closed if the bubble radius at contact angle of 90° exhibits a local minimum. Since contact angle of 90° can maintain for a period of time, a subsequent positive bubble growth rate-to-solidification rate ratio readily gives rise to an isolated pore. The pore can be elongated, expanded, shrunk, rippled or closed, depending on the bubble growth rate-to-solidification rate ratio. Manipulating the bubble growth rate or solidification rate to control the pore shape in solid is therefore provided.

1. Introduction

Study of pore formation in solid plays an important role in biological, engineering, geophysical and climate change sciences [1–3]. In nature, bubbles incorporated in rime, hailstones, and lake ice are well-known. Porosity of sea ices influences the surface elevation of the ice sheet, sun albedo, atmospheric heat and mass transfer, brine, enzymes and nutrients transport. For example, the primary production in the sea layer is affected by not only surface flooding but also temperature-dependent porosity of sea ice [4]. In the infiltration or surface layer, nutrients were supplied continuously whenever the snow density and thickness were sufficient to force the sea ice below sea level, namely, the ice surface flooded. Nutrients were supplied to the interior freeboard layer or sea level layer when the sea ice became permeable and the surface flooded. If these criteria failed, the nutrient supply was cut off until the surface flooded or the ice became permeable again.

Substances containing a number of pores have characteristics different from those of bulk substances, such as a low density and a large surface area. Therefore, they can be utilized as heat insulators, lightweight materials, catalysts, electrodes, vibration and acoustic energy absorption materials, impact energy absorption materials, and so on. Ice containing oxygen and nitrogen can therefore be used for food and fishery industries, and ozone for food preservation and sterilization [5,6]. Recently, in tissue engineering, creating artificial constructs for regeneration of new tissues has been a focus of many material scientists and medical professionals. A key component in tissue engineering for bone regeneration is the scaffold that serves as a template for cell interaction and formation of the bone-extracellular matrix to provide structural support to the newly formed tissues. Scaffolds for bone regeneration thus meet certain criteria, including the mechanical properties similar to those of the bone repair site, biocompatibility and biodegradability at a commensurate rate with remodeling. An interconnected porous structure is needed for scaffold to allow for tissue ingrowth and thus anchor the prosthesis to the surrounding bone, preventing loosening of implant and providing pathways for biofluids. Ekemen et al. [7] thus utilized a microbubbling process to generate controlled protein coated bubbles and then manipulate these to fabricate a variety of porous structures suitable for scaffolds and generic biomedical applications, tissue engineering, and biosensor coatings. Gu et al. [8] used a metal/gas eutectic unidirectional solidification method (GASAR process) [9–13] to prepare the lotus-type porous magnesium for the scaffold material. Magnesium alloys are degradable biomaterials with low densities and unique combination of good mechanical properties, biocompatibilities and biodegradation properties. The lotus-type porous metals that contain aligned long columnar pores in structural materials and functional materials have higher specific tensile strength in the direction parallel to the pore axis [14].

* Corresponding author. Tel.: +886 7 5254050; fax: +886 7 5254214.
E-mail addresses: pswei@mail.nsysu.edu.tw (P.S. Wei), macplayer.tw@yahoo.com.tw (S.Y. Hsiao).
[1] Tel.: +886 956335028.

0017-9310/$ - see front matter © 2012 Elsevier Ltd. All rights reserved.
http://dx.doi.org/10.1016/j.ijheatmasstransfer.2012.08.054

Nomenclature

A	a contact angle variable $A \equiv 1/\cos\theta_B$
Bo	Bond number, $Bo \equiv \rho g \widetilde{R}_0^2/\sigma$
H	sum of cap height and pore length below the solidification front.
M_{in}	mass flux of dissolved gas from liquid to bubble
p	pressure
r	cylindrical coordinate, $r \equiv \tilde{r}/\widetilde{R}_0$
R	bubble radius, $R \equiv \widetilde{R}/\widetilde{R}_0$
R_u	universal gas constant
s,$\tilde{s}$	solidification front displacement, $s \equiv \tilde{s}/\widetilde{R}_0$
t	time
T	temperature

Greek letters

σ	surface tension
ρ	density
θ	inclination angle
ω	area ratio of bubble cap

Subscripts

B	base
g	gas
0	initial state

Superscript

$\sim$	dimensional quantity

Pores, however, is also susceptible to stress concentration and leads to reduction in load capacity of the surface. In manufacturing processes, bubble incorporation in metals during casting or welding is a problematic issue, because it generally degrades the mechanical properties and impedes efficiency or functional properties of the products [15–18]. The resulting degradation of mechanical properties depends on the size distribution and volume fractions of pores.

To control or avoid porosity, mechanism of pore formation during solidification should be understood. Since gas solubility in solid is usually much less than that in liquid, gas is accumulated ahead of the solidification front [19]. Super-saturation therefore gives rise to nucleation of bubbles on the solidification front [20,21]. The emanated gas bubbles may either float away, or remain at the solidification front where they may be trapped in the solid as discrete pores, chains of pores, or gas tubes. The bubbles within the liquid are not often captured by the solid [22]. Therefore, bubble nucleation at the solidification front is the necessary condition for bubble entrapment and pore formation in solid.

Carte [23] observed pore formation in ice from water containing air. Bubble concentration increases and size decreased as the freezing rate increased. Bubbles were formed at the solidification front, when the superstation ratio was round 30 for freezing rates greater than 2 mm/min. Bari and Hallett [24] observed the formation and growth of bubbles during freezing of water with air and helium dissolved in it. Cylindrical gas tubes formed in the ice when the freezing rate was below 0.005 mm/s. Egg-shaped bubbles were trapped when the freezing rate was higher. Maeno [25] observed that when the growth rate of a bubble is larger it remains at the freezing interface, where it absorbs more gas and becomes larger. As it was large enough, it escaped upward. When the growth rate was less than the freezing rate, it was captured. When the growth rate was comparable, the bubble formed a cylindrical gas tube in the ice. Geguzin and Dzuba [26] also observed and proposed that a bubble is not captured, captured as an elongated inclusion, and isolated pore as the solidification front is, respectively, less, equal, and greater than the rate of displacement of the top surface of the growing bubble. Murakami and Nakajima [27] observed that columnar pores in water-carbon dioxide solutions are formed at low growth rates. The length of the columnar pores became shorter as the freezing rate increased or carbon dioxide concentration increased. Wei et al. [28] in-situ observed and measured pore shapes in ice during solidification of water containing oxygen and carbon dioxide gases. Pore formation can be divided into five regimes: (1) nucleation on the solidification front, (2) spherical growth, (3) solidification rate-controlled elongation, (4) disappearance of the bubbles, and (5) formation of the pores in solid. Yoshimura et al. [5] observed structural features of oxygen gas bubbles incorporated into a growing ice crystal at various ice growth rates and ambient pressures. As solidification rate increased, four patterns were observed: (a) egg-shaped bubbles, (b) egg-shaped bubbles and cylindrical bubbles, (c) cylindrical bubbles, and (d) bifurcated cylindrical bubbles. The measured diameter and interval decreased with increasing either the growth rate or ambient pressure.

In this work, a simple analysis is proposed to give a general insight into the pore shape resulted from a bubble entrapment by the solidification front. For simplicity without loss of generality, the model assumes that the pore shape is delineated by contact angel of the spherical bubble cap on the solidification front. The solidification rate and bubble growth rate are specified to avoid computations of heat transfer and fluid flow equations. Control of porosity formation to achieve desired properties of the materials is therefore provided.

2. System model and analysis

In this model, a pore in solid resulting from entrapment of a tiny bubble on a solidification front, located by displacement s measured from the initial solidification front, is illustrated in Fig. 1. The pore has a spherical cap beyond the solidification front.

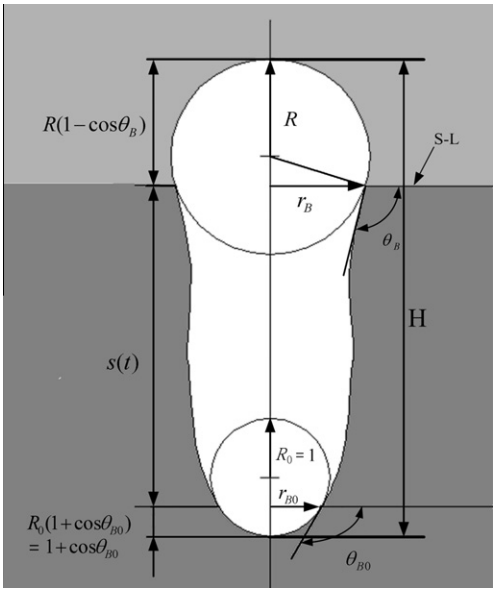

Fig. 1. Sketch of physical model and dimensionless coordinate system.

The dimensionless radius of the bubble cap is R, while contact angle and dimensionless base radius are θ_B and r_B, respectively. Radius, contact angle and base radius of the cap at the initial state are R_0, θ_{B0} and r_{B0}, respectively. It can be seen that the inclination angle of the pore at the solidification front is identical to the contact angle of the bubble cap. For simplicity without loss of generality, the major assumptions made are as follows:

1. The model system is axisymmetric.
2. The bubble cap in radius less than 100 μm is spherical. This is attributed to a very small Bond number [28].
3. Tracing the slope of the triple phase line of the bubble cap delineates the shape of the pore in solid [29]. It implies that the free surface in the pore is instantaneously solidified. It is unclear if a thin layer of liquid exists between the bubble and solidification front, as discussed by Maeno [25]. Even though a thin liquid layer exists, its thickness is around several nanometers [22,25]. Cooling gives rise to instant frozen of the free surface in the pore.
4. The bubble growth rate-to-solidification rate ratio is specified. Otherwise, determinations of gas pressure in the pore, and temperature fields in the solid and liquid are, respectively, required for calculating more realistic bubble growth rate and solidification rate.

With the above assumptions, the base radius of the bubble cap is given by (see Fig. 1)

$$r_B = R\sin\theta_B \tag{1}$$

The slopes of the bubble cap and pore in sold are continuous at the solidification front

$$\frac{ds}{dr_B} = -\tan\theta_B \tag{2}$$

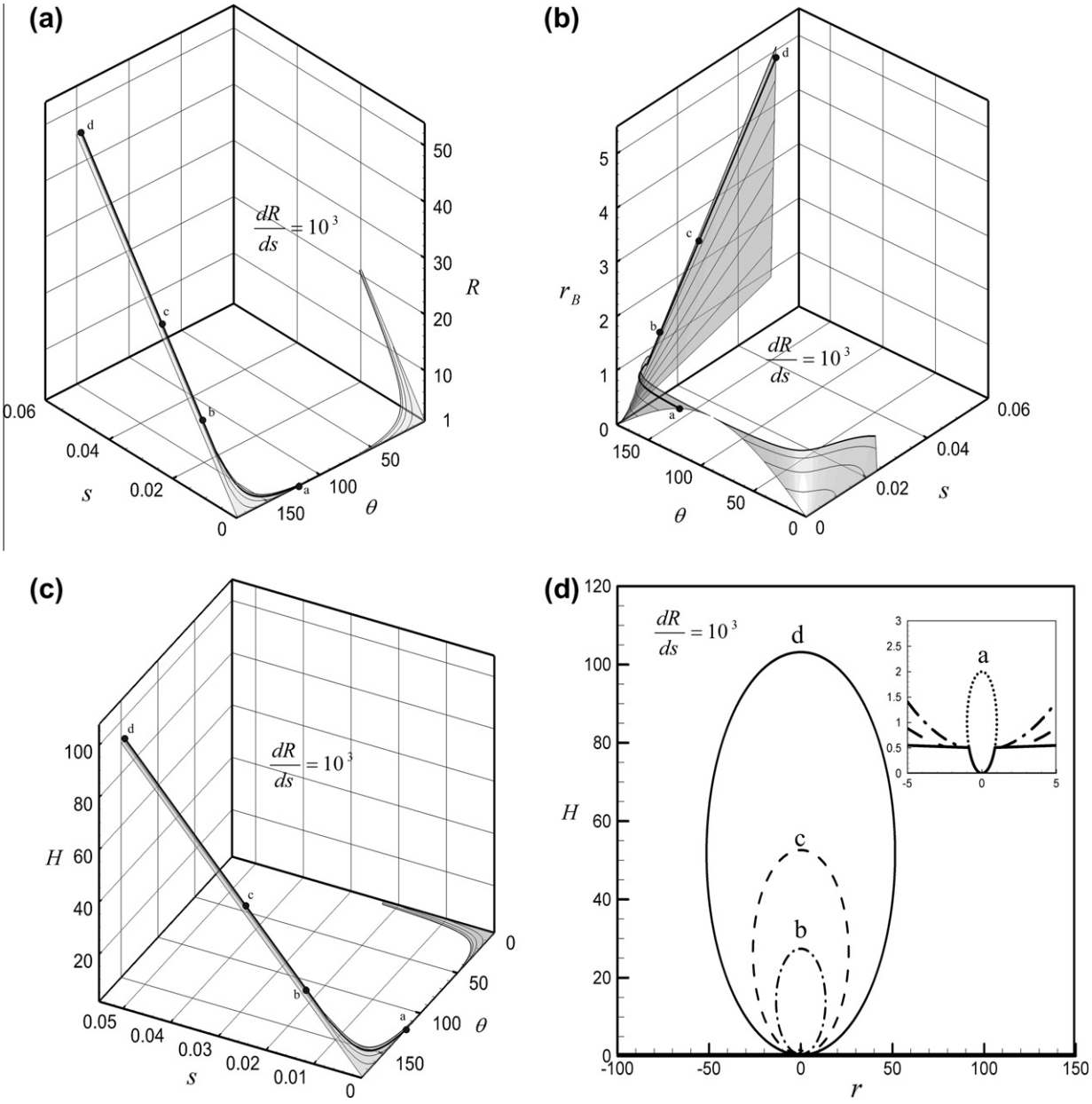

Fig. 2. (a) Bubble radius and (b) base radius of the bubble cap, and (c) total pore length as functions of solidification front displacement and contact angle, and (d) corresponding pore shape with $dR/ds = 10^3$.

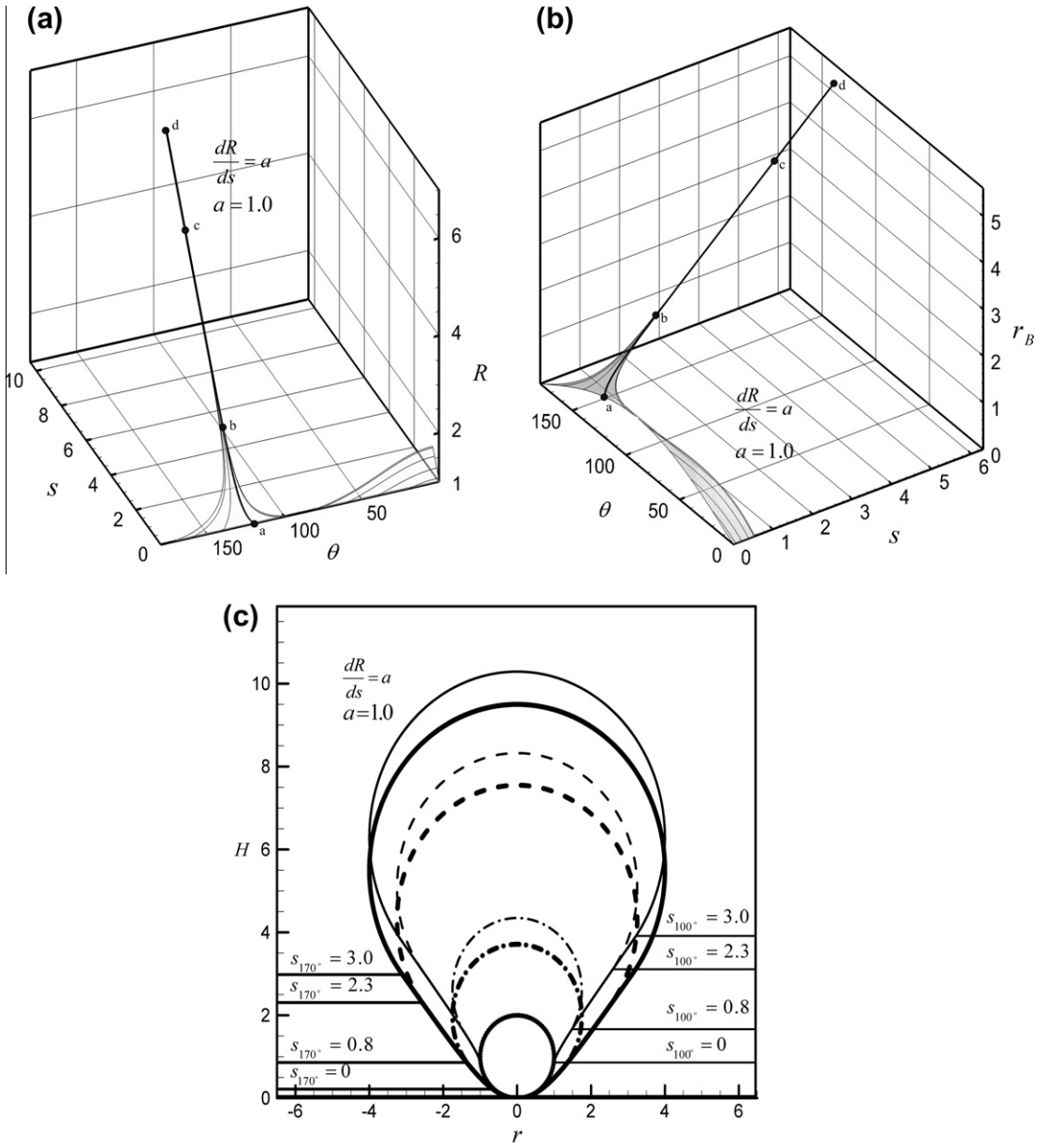

Fig. 3. (a) Bubble radius and (b) base radius of the bubble cap as functions of solidification front displacement and contact angle, and (c) corresponding pore shape with $dR/ds = 1$.

Substituting Eq. (1) into Eq. (2) leads to

$$\frac{dA}{ds} = -\frac{1}{R}\frac{dR}{ds}A^3 - \frac{1}{R}A^2 + \frac{1}{R}\frac{dR}{ds}A \tag{3}$$

where the contact angle variable $A \equiv 1/\cos\theta_B$. Interestingly, Eq. (3) is the Abel's equation of the first kind. It was numerically solved by using the Runge–Kutta method in this study. The initial condition is $A = 1/\cos\theta_{B0} \equiv A_0$ at $s = 0$. Selecting the bubble growth rate-to-solidification rate ratio $dR/ds = (dR/dt)/(ds/dt)$ and substituting contact angle from Eq. (3), the pore shape can be predicted from Eq. (1). Since contact angle of 90° corresponding to $A \to \infty$, Eq. (3) for a finite dR/ds reduces to

$$\frac{dA}{ds} = -\frac{1}{R}\frac{dR}{ds}A^3 \tag{4}$$

Integrating Eq. (4) leads to

$$A = \frac{\pm 1}{\sqrt{\ln\left(\frac{R}{R_{90}}\right)^2}} \tag{5}$$

where bubble radius at the contact angle of 90°, R_{90}, should be minimal to avoid negative value in the square root. It is noted that Eq. (4) is invalid in the case of a stationary bubble for $dR/ds \to 0$, because Eq. (4) cannot be deduced from Eq. (3). To estimate a rather realistic bubble growth rate, conservation of mass for gas is needed [28]. Changing rate of the mass in the pore is identical to the mass flux across the cap surface. In the early stage, it is given by

$$\frac{d}{dt}\left(\frac{4}{3}\pi\tilde{R}^3\rho_g\right) = 4\pi\tilde{R}^2\omega M_{in} \tag{6}$$

Assuming that the variation of gas density with time is much less than that of bubble radius to the third power and substituting the equation of state, Eq. (6) reduces to

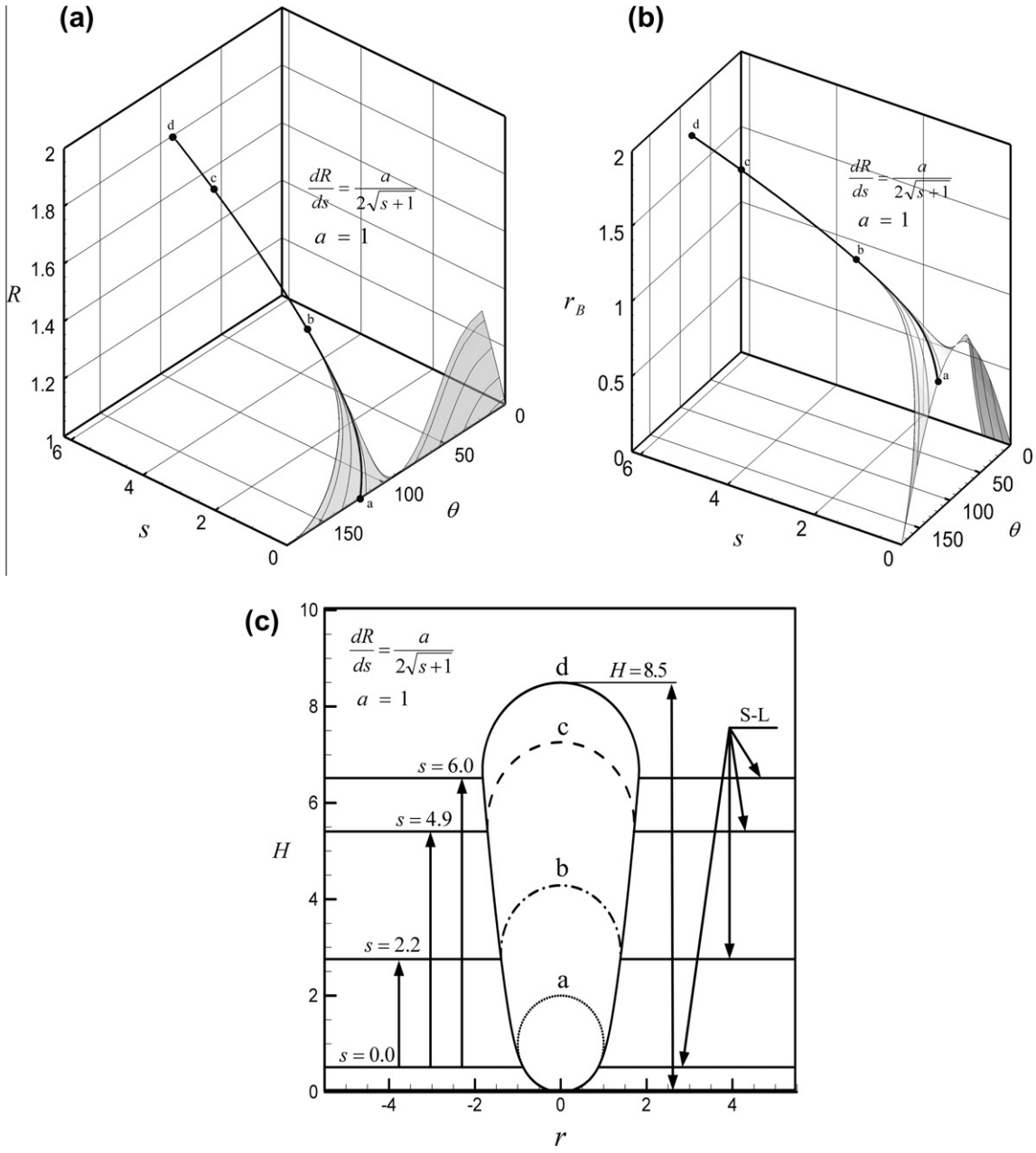

Fig. 4. (a) Bubble radius and (b) base radius of the bubble cap as functions of solidification front displacement and contact angle, and (c) corresponding pore shape with $dR/ds = 1/(2\sqrt{s+1})$.

$$\frac{d}{dt}\left(\frac{4}{3}\pi\widetilde{R}^3\right) \approx 4\pi\widetilde{R}^2\omega M_{in}\left(\frac{R_u T_g}{p_g}\right) \tag{7}$$

Substituting the Young–Laplace equation, Eq. (7) becomes

$$\frac{d}{dt}\left(\frac{4}{3}\pi\widetilde{R}^3\right) \sim 4\pi\widetilde{R}^2\omega M_{in}R_u T_g\left(\frac{\widetilde{R}}{\sigma}\right) \tag{8}$$

Since mass flux across the cap surface $M_{in} \sim 1/R^2$, Eq. (8) leads to

$$R \sim \sqrt{t} \sim \sqrt{s} \tag{9}$$

where time is assumed to be proportional to displacement of the solidification front. In fact, the bubble can grow in different power of time for different working parameters and stages [30]. Substituting Eq. (9), a typical expression of the bubble growth rate-to-solidification rate ratio is thus given by

$$\frac{dR}{ds} \sim \frac{1}{\sqrt{s}} \tag{10}$$

3. Results and discussion

In this study, the pore shape resulted from a tiny bubble captured by a solidification front is predicted. The pore shape is determined by bubble radius and contact angle of the cap. An isolated or enclosed pore takes place as the contact angle becomes zero. The contact angle required for calculating the pore shape is found to be governed by the well-known non-linear Abel's equation of the first kind in terms of displacement of the solidification front. The controlling parameter is only the bubble growth rate-to-solidification rate ratio, implying a relative variation between bubble growth rate and solidification rate. The solutions of Abel's equation can also be considered as the zeroth approximation to pore

formation resulted from a bubble captured by a solidification front. To have a more realistic bubble shape, mass, momentum, and species transport and physic-chemical equilibrium on the cap are needed [31]. The solidification front displacement or fictitious time is chosen as the independent variable, so that thermal energy equations of solid and liquid are not to be solved.

A phase surface for bubble radius, which is a function of solidification front displacement and contact angle, during freezing with a high bubble growth rate-to-solidification rate ratio $dR/ds = 10^3$ is shown in Fig. 2(a). It can be considered as a bubble grows on a stationary solidification front. Each line on the phase surface represents the path of a pore growth specified by a given initial contact angle. Bubble radius evidently increases in the course of solidification. There exist two groups of phase surface distinguished by contact angle of 90° at the minimal bubble radius. For an initial contact angle less than 90° contact angles of the cap are smaller than 90° in the course of solidification. Contact angles of the cap, however, maintain greater than 90° during solidification for the initial contact angle greater than 90°. Regardless of initial contact angles, contact angles approach asymptotic constant values, which are close to zero and 180°, respectively. Inclination angle of the pore wall is therefore constant in the upper region.

Fig. 2(b) shows base radius of the cap as a function of solidification front displacement and contact angle. Since base radius vanishes, the pore with contact angles less than 90° is entrapped as an isolated pore. However, the pore having contact angles greater than 90° remains opening. Fig. 2(c) indicates that the pore with contact angles less than 90° is entrapped very rapidly due to small and nearly constant pore length. On the other hand, the pore length for contact angles greater than 90° monotonically increases

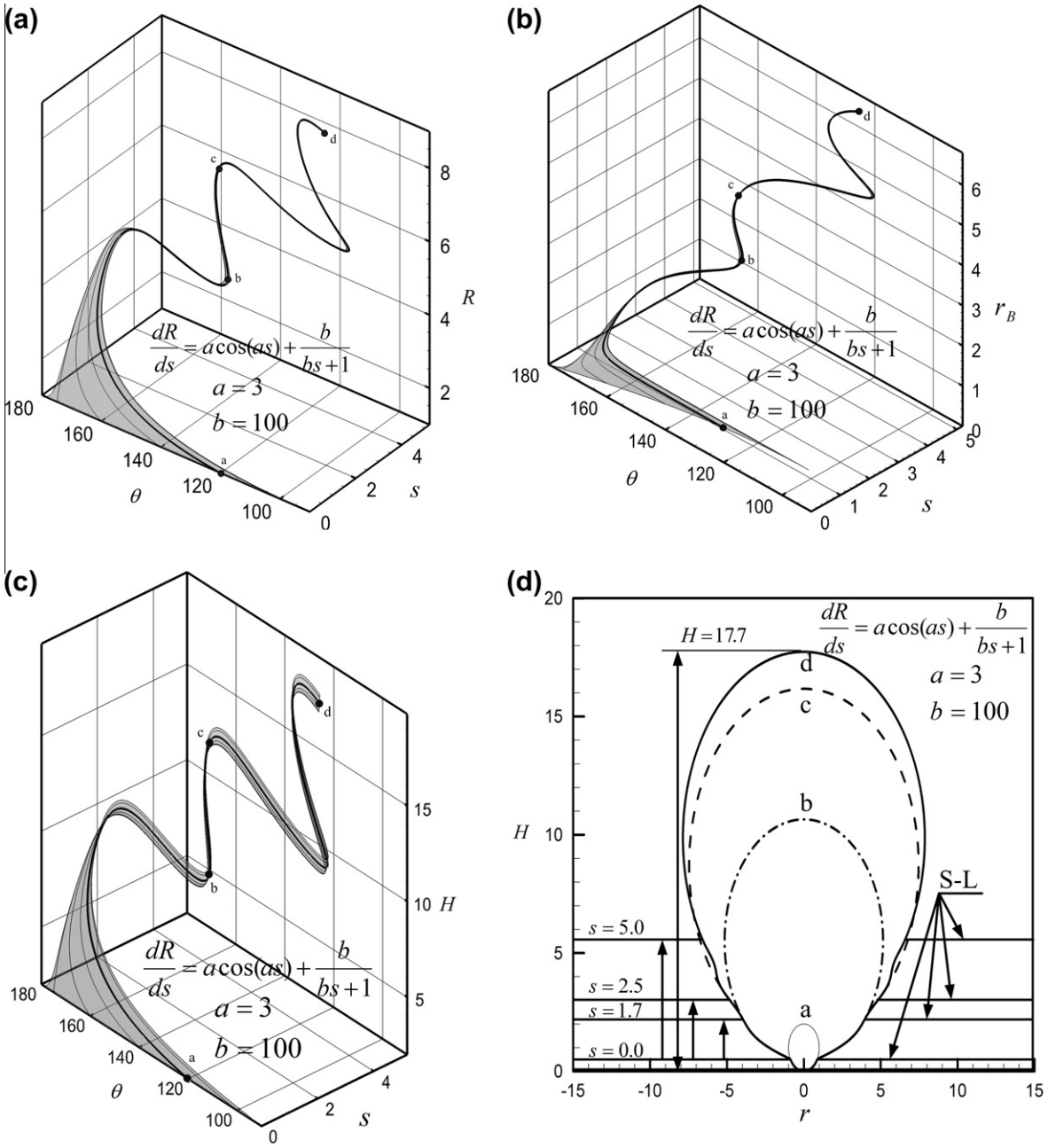

Fig. 5. (a) Bubble radius and (b) base radius of the bubble cap, and (c) total pore length as functions of solidification front displacement and contact angle, and (d) corresponding pore shape with $dR/ds = 3\cos(3s) + 100/(100s + 1)$.

during solidification. The pore shape therefore is not closed, as can be seen in Fig. 2(d).

Radii of the bubble and its cap base as functions of solidification front displacement and contact angle for $dR/ds = 1$ are, respectively, shown in Figs. 3(a) and (b). Similarly, contact angles approach an asymptotic constant, which is independent of initial contact angle. In the early stage contact angles decreases or increases, depending on if the initial contact angle is greater or smaller than the asymptotic value. Referring to previous Fig. 2(a) or (b), it shows that the asymptotic contact angle decreases with the bubble growth rate-to-solidification rate ratio. Moreover, a smaller bubble growth rate-to-solidification rate ratio results in a more rapid closure of the pore. A lower initial contact angle increases contact angles in the early stage, and the corresponding pore shape is shown in Fig. 3(c). The pore shape is different, even though asymptotic contact angle is the same. The pore maintains opening.

In the case of more realistic bubble growth rate-to-solidification rate ratio $dR/ds = 1/(2\sqrt{s+1})$, as derived in Eq. (10), radii of bubble and cap base as functions of solidification front displacement and contact angle are shown in Fig. 4(a) and (b), respectively. The corresponding pore shape is shown in Fig. 4(c). Since increasing rate of bubble radius decreases in the course of solidification, contact angle approaches 90°, leading to a narrow pore. This agrees with experimental observations [23,24], showing that a narrow pore results for a high solidification rate. The pore maintains open, because more time is needed to reach 90°. Fig. 5(a) through (c) show that bubble radius, cap base radius, and pore length oscillate in the course of solidification. The pore is thus in a wavy shape, as shown in Fig. 5(d). Even though the bubble growth rate-to-solidification rate ratio oscillates, the pore is not closed. This is because contact angles do not approach 90°.

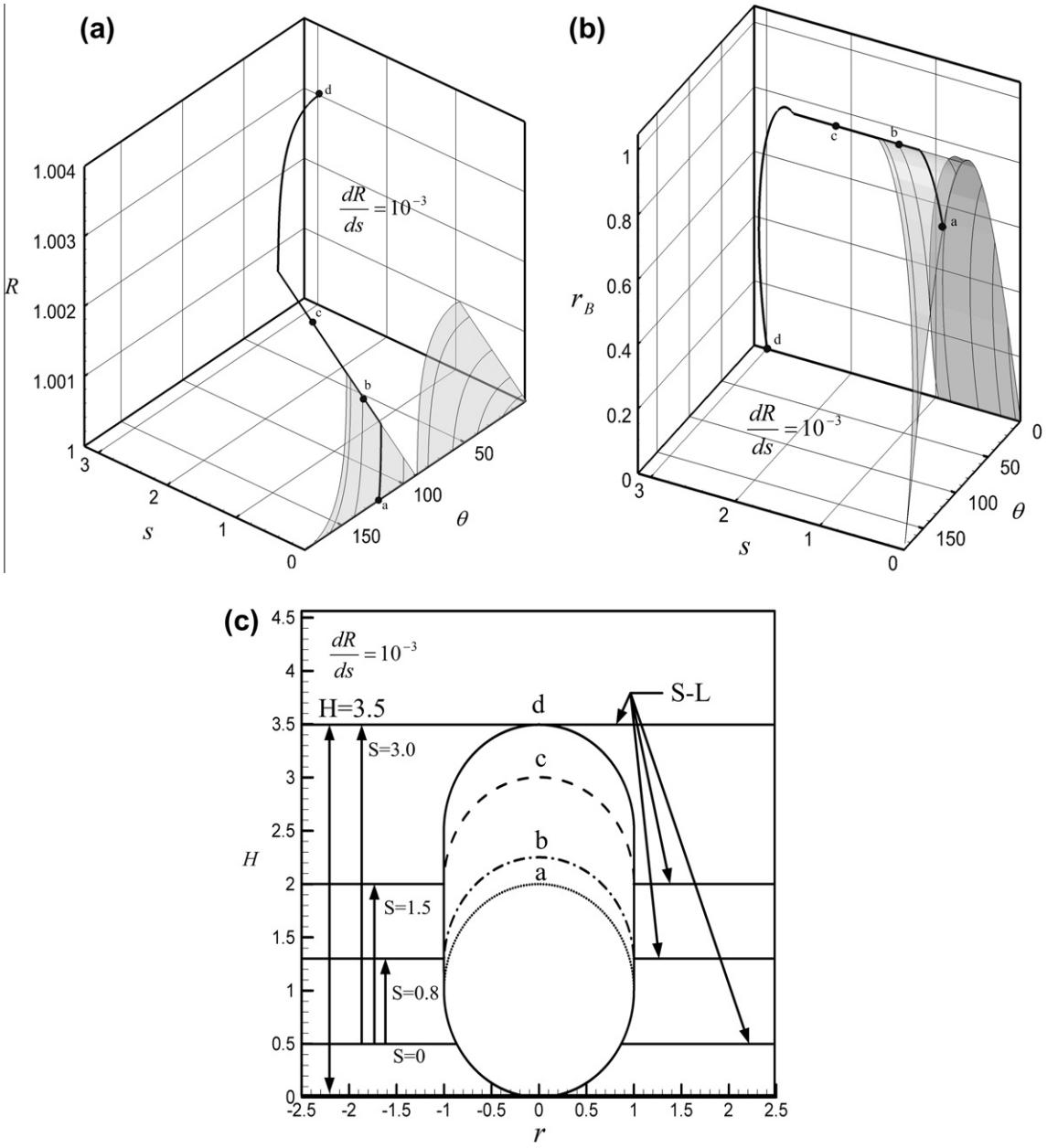

Fig. 6. (a) Bubble radius and (b) base radius of the bubble cap as functions of solidification front displacement and contact angle, and (c) corresponding pore shape with $dR/ds = 10^{-3}$.

For a bubble growth rate-to-solidification rate ratio $dR/ds = 0.001$ or infinitesimal, contact angle decreases during solidification, as shown in Fig. 6(a). A small bubble growth rate-to-solidification rate ratio can be considered as a nearly stationary bubble passed by a solidification front. The pore subject to an infinitesimal bubble growth rate-to-solidification rate ratio can be closed, even though contact angles are greater than 90°. This is because contact angle approaches and reaches 90° and maintains a period of time. As long as bubble radius increases as contact angles are slightly less than 90°, the pore becomes closed. Since displacement of the solidification front implies time, the decrease in contact angle during freezing is confirmed by measurements [28]. The variation of cap base radius with displacement of the solidification front is shown in Fig. 6(b). Development of the pore shape and its entrapment as an isolated pore is seen in Fig. 6(c).

Bubble radius and contact angle affected by oscillatory $dR/ds = 0.04\sin(0.4s)$ are shown in Fig. 7(a). In view of the small and positive bubble growth rate-to-solidification rate ratio, contact angle decreases and bubble radius increases in the early stage. Bubble radius, however, becomes decreased, namely, $dR/ds < 0$ for $s > 7.8$ corresponding to contact angles slightly greater than 90°. In contrast to previous Fig. 5(d), the solidification front can reach contact angle of 90° and maintain a period of time, where bubble radius exhibits a local minimum. As soon as bubble radius increases further, the pore becomes closed, as shown in Fig. 7(b). In reality, gas pressure usually decreases with time, leading to an increase in bubble radius in order to satisfy Young–Laplace equation. The length of an isolated pore subject to a nonzero bubble growth rate-to-solidification rate ratio cannot be accurately determined. This is because the pore becomes closed as long as bubble radius

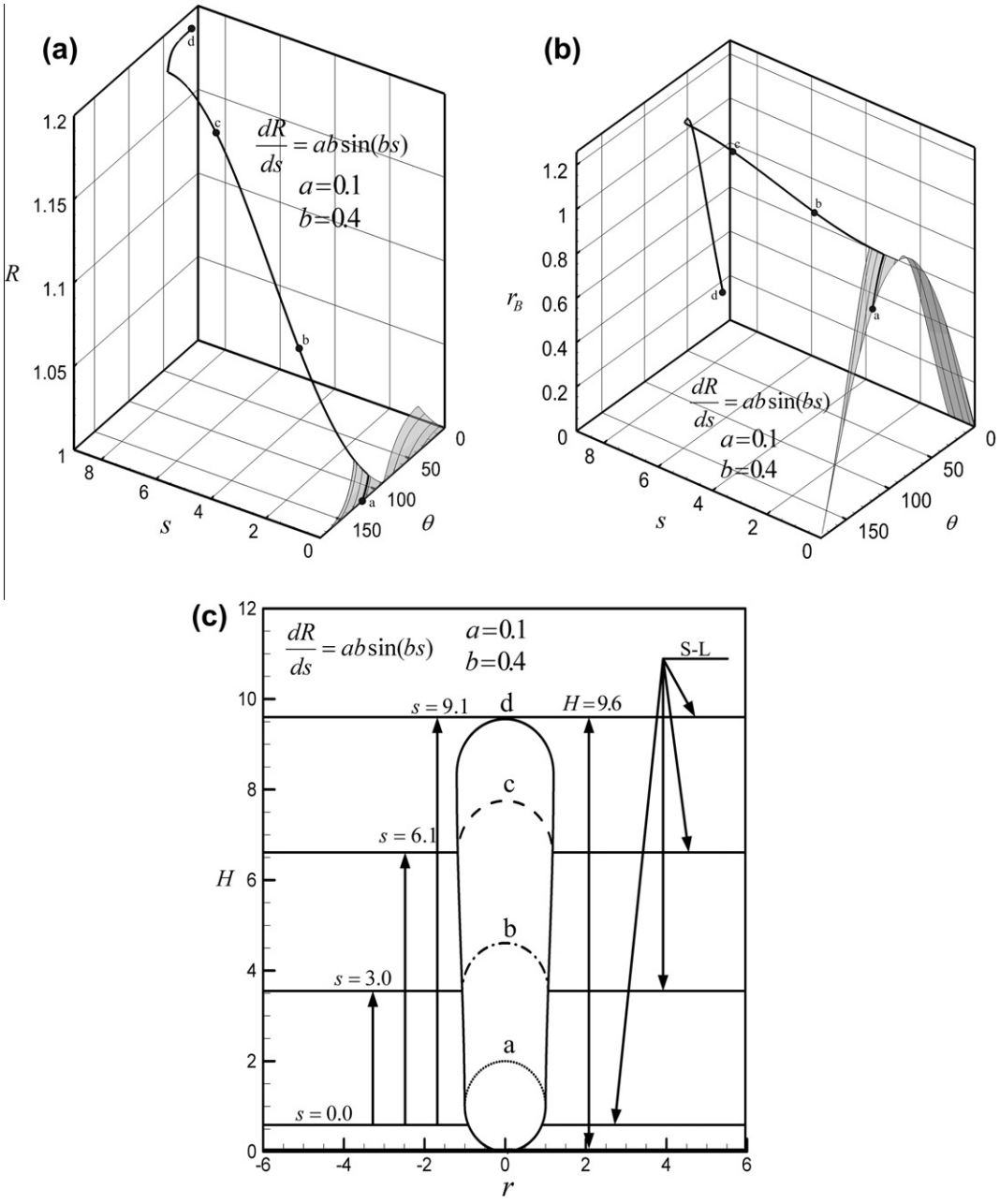

Fig. 7. (a) Bubble radius and (b) base radius of the bubble cap as functions of solidification front displacement and contact angle, and (c) corresponding pore shape with dR/ds = 0.04 sin(0.4s).

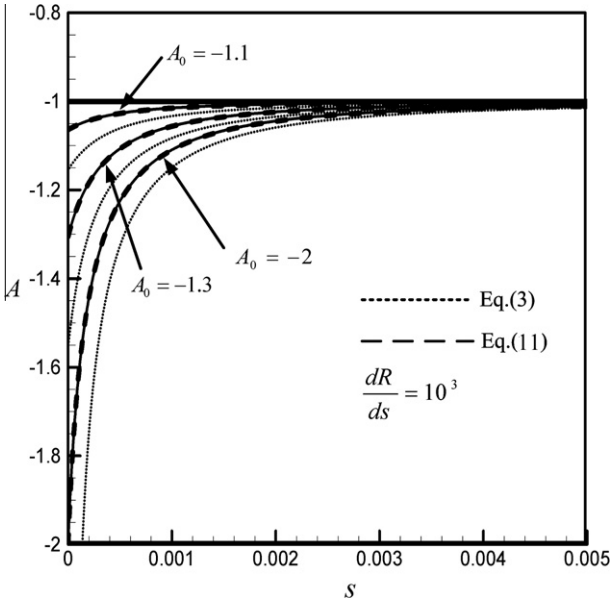

Fig. 8. A comparison of predicted contact angle variable between Eq. (3) and asymptotic Eq. (11) for high dR/ds = 10^3.

slightly increases in the course of long duration time at contact angle of 90°. Development of the pore is shown in Fig. 7(c). It can be seen the pore is closed at solidification front displacement of around 9.1. Contact angle of 90° is maintained during a period of time or solidification front displacement between 1 and 8.

To confirm the numerical results, asymptotic results are introduced. For $dR/ds \gg 1$ Eq. (3) becomes a special form of the Landau equation [32]. Its solution is given by

$$A = \frac{A_0}{\sqrt{A_0^2 + (1 - A_0^2)e^{-2\tau}}} \tag{11}$$

where the time-like independent variable $\tau \equiv \ln R$. Fig. 8 shows good agreement between Eqs. (3) and (11). The present model is derived from a geometrical analysis. Provided that the bubble growth rate-to-solidification rate ratio is realistically predicted or measured, this work subject to small Bond numbers can be applied to find general and accurate results.

4. Conclusions

The conclusions drawn are the following:

1. The three-dimensional pore shape, which can be elongated, expanded, shrunk, rippled or closed, depends on the bubble growth rate-to-solidification rate ratio, or relative variation between bubble growth rate and solidification rate.
2. The pore is rapidly closed for contact angles less than 90°. The pore maintains open for contact angles greater than 90° subject to high bubble growth rate-to-solidification rate ratios.
3. In the case of nonzero bubble growth rate-to-solidification rate ratios, the necessary condition for an isolated pore is that bubble radius exhibits a local minimum at the contact angle of 90°. How to reach contact angle of 90° and increase bubble radius at this contact angle from controlling of the bubble growth rate-to-solidification rate ratio is critical.
4. The length of an isolated pore subject to a nonzero bubble growth rate-to-solidification rate ratio cannot be accurately determined. This is because the pore becomes closed as long as bubble radius slightly increases in the course of long duration time at contact angle of 90°.
5. Pore is closed for a zero bubble growth rate-to-solidification rate ratio.
6. The pore is susceptible to closure if the bubble growth rate-to-solidification rate ratio oscillates near contact angle of 90°, or the bubble growth rate-to-solidification rate ratio is infinitesimal.
7. A well-known criterion, stating that a pore is closed as long as solidification rate is greater than bubble growth rate, is incorrect.
8. The pore becomes a rippled wormhole, when either the bubble or the solidification front oscillates.
9. Accounting for mass, momentum, energy and species transport and their interfacial balances is essentially required to evaluate more realistic bubble growth rate and solidification rate, leading to a predictable pore shape.
10. The present model valid for small Bond numbers is derived from a geometrical analysis. Provided that the bubble growth rate-to-solidification rate ratio is realistically known, this study thus can be used to obtain rather general and accurate results.

Acknowledgment

This work was financially supported by the project NSC 97-2221-E-110-071-MY3 from National Science Council, Taiwan, Republic of China.

References

[1] B. Loose, L.A. Miller, S. Elliott, T. Papakyriakou, Sea ice biogeochemistry and material transport across the frozen interface, Oceanography 24 (2011) 202–218.
[2] H. Eicken, C. Bock, R. Wittig, H. Miller, H.-O. Poertner, Magnetic resonance imaging of sea-ice pore fluids: methods and thermal evolution of pore microstructure, Cold Reg. Sci. Technol. 31 (2000) 207–225.
[3] C.H. Fritsen, V.I. Lytle, S.F. Ackley, C.W. Sullivan, Autumn bloom of Antarctic pack-ice algae, Science 266 (1994) 782–784.
[4] K.R. Arrigo, D.L. Worthen, M.P. Lizotte, P. Dixon, G. Dieckmann, Primary production in Antarctic sea ice, Science 276 (1997) 394–397.
[5] K. Yoshimura, T. Inada, S. Koyama, Growth of spherical and cylindrical oxygen bubbles at an ice–water interface, Cryst. Growth Design 8 (2008) 2108–2115.
[6] T. Inada, T. Hatakeyama, F. Takemura, Gas-storage ice grown form water containing microbubbles, Int. J. Refrigeration 32 (2009) 462–471.
[7] Z. Ekemen, H. Chang, Z. Ahmad, C. Bayram, Z. Rong, E.B. Denkbas, Fabrication of biomaterials via controlled protein bubble generation and manipulation, Biomacromolecules 12 (2011) 4291–4300.
[8] X.N. Gu, W.R. Zhou, Y.F. Zheng, Y. Liu, Y.X. Li, Degradation and cytotoxicity of lotus-type porous pure magnesium as potential tissue engineering scaffold material, Mater. Lett. 64 (2010) 1871–1874.
[9] V. I. Shapovalov, U. S. Patent No. 5181,549 (Jan. 26, 1993).
[10] J.S. Park, S.K. Hyun, S. Suzuki, H. Nakajima, Effect of transference velocity and hydrogen pressure on porosity and pore morphology of lotus-type porous copper fabricated by a continuous casting technique, Acta Mater. 55 (2007) 5646–5654.
[11] Y. Liu, Y.X. Li, J. Wan, H.W. Zhang, Evaluation of porosity in lotus-type porous magnesium fabricated by metal/gas eutectic unidirectional solidification, Mater. Sci. Eng. A. 402 (2005) 47–54.
[12] M. Tane, H. Nakajima, Influence of ultrasonic agitation on pore formation and growth during unidirectional solidification of water-carbon dioxide solution, Mater. Trans. 47 (2006) 2183–2187.
[13] M.C. Cox, A.V. Anilkumar, R.N. Grugel, C.P. Lee, Effect of step-wise change in processing pressure on isolated pore growth during controlled directional solidification in small channels, J. Cryst. Growth 311 (2009) 327–336.
[14] H. Nakajima, Fabrication, properties and application of porous metals with directional pores, Progress Mater. Sci. 52 (2007) 1091–1173.
[15] S. Kou, Welding Metallurgy, 2nd edition., Wiley, New York, 2003.
[16] M. Pastor, H. Zhao, R.P. Martukanitz, T. DebRoy, Porosity, underfill and magnesium loss during continuous wave Nd:YAG laser welding of thin plates of aluminum alloys 5182 and 5754, Weld. J. 78 (1999) 207s–216s.
[17] J.H. Lau, S.W.R. Lee, Chip Scale Package, CSP: Design, Materials, Process, Reliability, and Applications, McGraw-Hill, New York, 1999.
[18] P.B. Oliete, J.I. Peña, Study of the gas inclusions in $Al_2O_3/Y_3Al_5O_{12}$ and $Al_2O_3/Y_3Al_5O_{12}/ZrO_2$ eutectic fibers grown by laser floating zone, J. Cryst. Growth 304 (2007) 514–519.

[19] A.I. Fedorchenko, A.A. Chernov, Exact solution of the problem of gas segregation in the process of crystallization, Int. J. Heat Mass Transfer 46 (2003) 915–919.
[20] P.S. Wei, C.C. Huang, K.W. Lee, Nucleation of bubbles on a solidification front-experiment and analysis, Metall. Mater. Trans. B 34 (2003) 321–332.
[21] A.A. Chernov, A.A. Pil'nik, Melt cavitation at its volumetric crystallization, Int. J. Heat Mass Transfer 55 (2012) 294–301.
[22] J.C.T. Kao, A.A. Golovin, S.H. Davis, Particle capture in binary solidification, J. Fluid Mech. 625 (2009) 299–320.
[23] A.E. Carte, Air bubbles in ice, Proc. Phys. Soc. London 77 (1961) 757–768.
[24] S.A. Bari, J. Hallett, Nucleation and growth of bubbles at an ice–water interface, J. Glaciol. 13 (1974) 489–520.
[25] N. Maeno, Air bubble formation in ice crystals, in: Physics of Snow and Ice, Proc., Vol. 1, Part 1, H. Oura, (Ed.) Hokkaido University, Sapporo, Japan, 1967 pp. 207–218.
[26] Ya.E. Geguzin, A.S. Dzuba, Crystallization of a gas-saturated melt, J. Cryst. Growth. 52 (1981) 337–344.
[27] K. Murakami, H. Nakajima, Formation of pores during unidirectional solidification of water containing carbon dioxide, Mater. Trans. 43 (2002) 2582–2588.
[28] P.S. Wei, C.C. Huang, Z.P. Wang, K.Y. Chen, C.H. Lin, Growths of bubble/pore sizes in solid during solidification – an in situ measurement and analysis, J. Cryst. Growth 270 (2004) 662–673.
[29] P.S. Wei, C.Y. Ho, An analytical self-consistent determination of a bubble with a deformed cap trapped in solid during solidification, Metall. Mater. Trans. B 33 (2002) 91–100.
[30] D.E. Rosner, M. Epstein, Effects of interface kinetics, capillarity and solute diffusion on bubble growth rates in highly supersaturated liquids, Chem. Eng. Sci. 27 (1972) 69–88.
[31] P.S. Wei, Y.K. Kuo, S.H. Chiu, C.Y. Ho, Shape of a pore trapped in solid during solidification, Int. J. Heat Mass Transfer 43 (2000) 263–280.
[32] P.G. Drazin, W.H. Reid, Hydrodynamic Stability, Cambridge University Press, 1981.